Arch. Metall. Mater. **69** (2024), 2, 783-786

DOI: https://doi.org/10.24425/amm.2024.149810

K. CHADHA[1,2*], Y. TIAN[3], J.G. SPRAY[2], C. ARANAS JR.[1]

EFFECT OF HIP TREATMENT ON THE EVOLUTION OF TEXTURE AND MICROSTRUCTURE OF LBPF FABRICATED PURE Ni

Microstructure and texture analysis were conducted employing electron backscatter diffraction (EBSD) technique on laser powder bed fusion (LPBF) fabricated pure Ni. The texture analysis of the hot isostatic pressed (HIP) and as-printed (AP) samples were done utilizing orientation distribution function (ODF) maps. The AP sample comprises mostly of <110>||BD fiber texture with insignificant presence of twins. In contrast, the HIP sample has <111>||BD grains. It was found that the development of the texture <111>||BD was due to the deformation linked to the HIP process. In addition, HIP generated a substantial fraction of Σ3 coincident site lattice boundaries (CSL) because of pure Ni which is a medium stacking fault energy (SFE) element.

Keywords: Pure Ni; LPBF; Additive Manufacturing; HIP; Texture

1. Introduction

In recent years, additive manufacturing (AM) has become popular in manufacturing components with improved functionality [1]. With the use of layer-by-layer deposition technique, AM technology is capable of producing complex shaped products with other advantages like reduced manufacturing steps and reduced material consumption. Among various techniques in AM manufacturing, LPBF has gained greatest attention due to the fact that it has ability to produce complex shapes and geometries [2-4]. LPBF has been widely used to manufacture various alloys e.g., steels, titanium alloys, HEA alloys, Al alloys etc. and have found their application in aerospace, defense, automotive, oil and gas sectors, etc. [5-9].

Pure Ni has an excellent corrosion endurance against caustic soda and other alkaline solutions. It is also able to withstand halogen gas and non-oxidizing acids because of which it is used for various devices such as heat exchangers used in the soda industry and reaction towers and tanks. Pure Ni also has low electrical resistance, good weldability, good workability and due to this it is also used as soda electrolytic electrodes, plating electrodes, battery parts etc. [10-12].

There is no literature present investigating fabrication of pure Ni using LPBF techniques. The present research is focused on studying the effect of HIP treatment on LPBF manufactured pure Ni. It is envisaged that studying the microstructure and texture would open opportunities for commercially manufacturing pure Ni.

2. Materials and methods

The samples of pure Ni were fabricated at voestalpine Additive Manufacturing Center Ltd., Mississauga, Ontario, Canada (vAMC) using LPBF utilizing an EOS M290 machine. Gas atomized powders were used with diameters between 15 and 25 µm and a Hall flow rate of 14.89 s per 50 g. LPBF was carried out as per the parameters enlisted in TABLE 1. The parameters were selected after conducting multiple trails with the EOS M290 machine. These parameters (TABLE 1) lead to printing

TABLE 1

Parameters for LPBF process

Parameters	Values
Layer Thickness	60 µm
Hatch distance	200 µm
Laser power	350 W
Rotation angle	55°
Laser speed	1000 mm/s
Volumetric energy density	30 to 40 J/mm^3

[1] UNIVERSITY OF NEW BRUNSWICK FREDERICTON, DEPARTMENT OF MECHANICAL ENGINEERING, NEW BRUNSWICK E3B 5A3, CANADA
[2] UNIVERSITY OF NEW BRUNSWICK FREDERICTON, PLANETARY AND SPACE SCIENCE CENTRE, NEW BRUNSWICK E3B 5A3, CANADA
[3] VOESTALPINE ADDITIVE MANUFACTURING CENTRE LTD. MISSISSAUGA, ONTARIO L5N 7Y3 CANADA

* Corresponding author: k.chadha@unb.ca; kchadha1987@gmail.com

the Pure Ni with minimum porosity. The Printing occurred in argon atmosphere to minimize oxidation.

Cubic samples (10 mm) were fabricated for microstructural analysis. The samples as-printed (AP) were subjected to hot isostatic pressing (HIP) [13] in accordance with the conditions given in TABLE 2. The cooling was carried out by quenching of nitrogen at 5-6 bar up to 65°C. Argon gas atmosphere was used during the heat treatment process.

TABLE 2

Parameters for HIP Process

Treatment	Temperature	Time	Pressure
HIP	1163°C	3h	~1 Mbar
Annealing	900°C	2h	Not Applicable

Cubic samples of AP and HIP were polished utilizing silicon carbide papers (grit size ranging 400-1200) and then diamond suspensions (starting from 3 to 1 µm). The final polishing was achieved with a Buehler Vibromet 2 polisher with silica suspension of 0.02 µm for 24 hours. To obtain electron backscatter diffraction (EBSD) data, Hitachi SU-70 field emission electron microscope was used. Post processing such as texture analysis and Orientation Distribution Function (ODF) was done with Channel 5™ software (Oxford Instruments, UK). BD (building direction) were used during analysis as a reference direction for all samples.

3. Results and discussions

Figs. 1 and 2 show the crystallographic texture of the as printed and HIP treated samples representing orientation distribution function (ODF) maps at $\varphi_2 = 0°$ and $\varphi_2 = 45°$ sections and texture component maps. It should be noted that the BD (building direction) is utilized as the reference direction for the entire texture representation.

It can be seen from Fig. 1, the grain morphology is mainly equiaxed grains with the average grain size is about 2.87 µm. There are localized areas with fine-grained microstructures (below 1 µm) that can develop as a result of static and/or dynamic recrystallization. The driving force may be because of residual stresses generated by rapid post printing solidification [14,15]. Fig. 1a present the grain boundary map for the AP sample. Low angle grain boundaries (LAGBs) fraction is 38.2% and that of high angle grain boundaries is 61.8% (HAGBs). The grain boundaries are determined to be HAGBs if there is a misorientation of more than 15°. Conversely, LAGBs are characterized by misorientations ranging from 2° to 15° and can be linked to the density of dislocations within the material.

The texture in the as printed pure Ni is weak with 4.12 being the maximum intensity factor. At $\varphi_2 = 0°$, there is dominance of fiber textures <111>||BD and <110>||BD, as validated by Fig. 1b (ODF map). Likewise, at $\varphi_2 = 45°$, fiber texture <110>||BD and <100>||BD are in dominance. Fig. 1(c-e) shows the ODF map of different fiber texture in the material. It can be seen that <110>||BD fiber texture is dominant with the fraction of 33.1%. The other fiber texture has smaller fractions, like <111>||BD (22.1%) and <100>||BD (24.5%) fiber texture.

Fig. 2, shows the EBSD maps of HIP treated sample. The grain morphology is mostly polygonal with average grain size is about 5.87 µm. The substantial presence of twins in the microstructure can be observed due to the application pressure in HIP process. LAGBs fraction is 8.2% and that of HAGBs is 91.8%. Due to the application of pressure at an elevated temperature

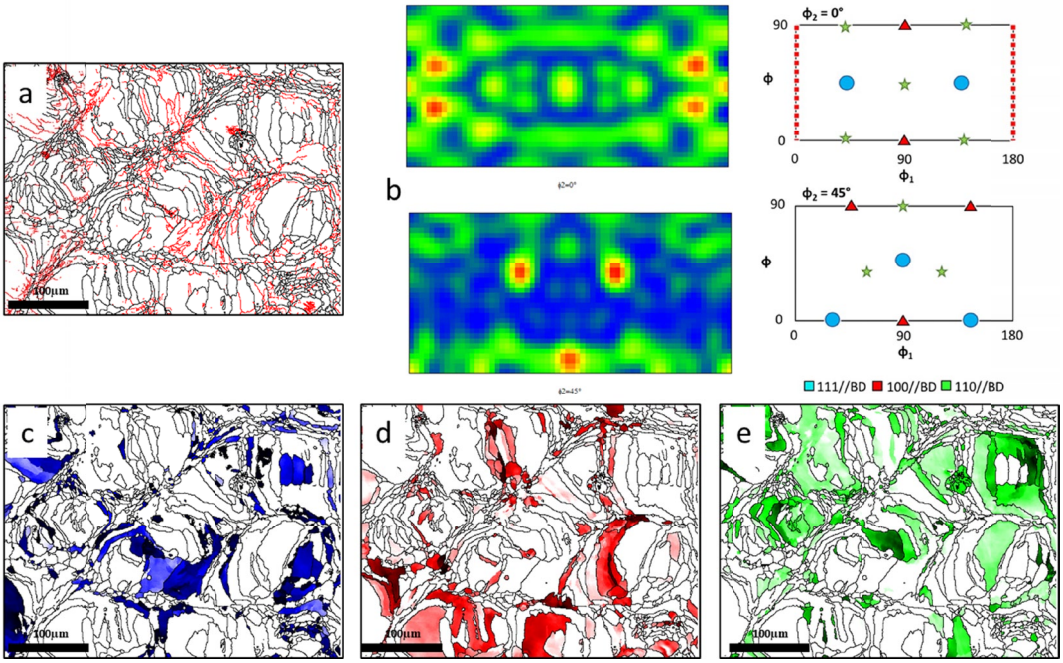

Fig. 1. The following figures are for as printed pure Ni sample, a) The grain boundary map with LAGB (red lines) and HAGB (black lines). b) The ODF maps showing the section with $\varphi_2 = 0°$ (top) and $\varphi_2 = 45°$ (bottom). (The interpretation of the ideal orientations of ODF maps is shown in this figure legend. (c) 111 fiber, (d) 100 fiber and (d) 110 fiber texture

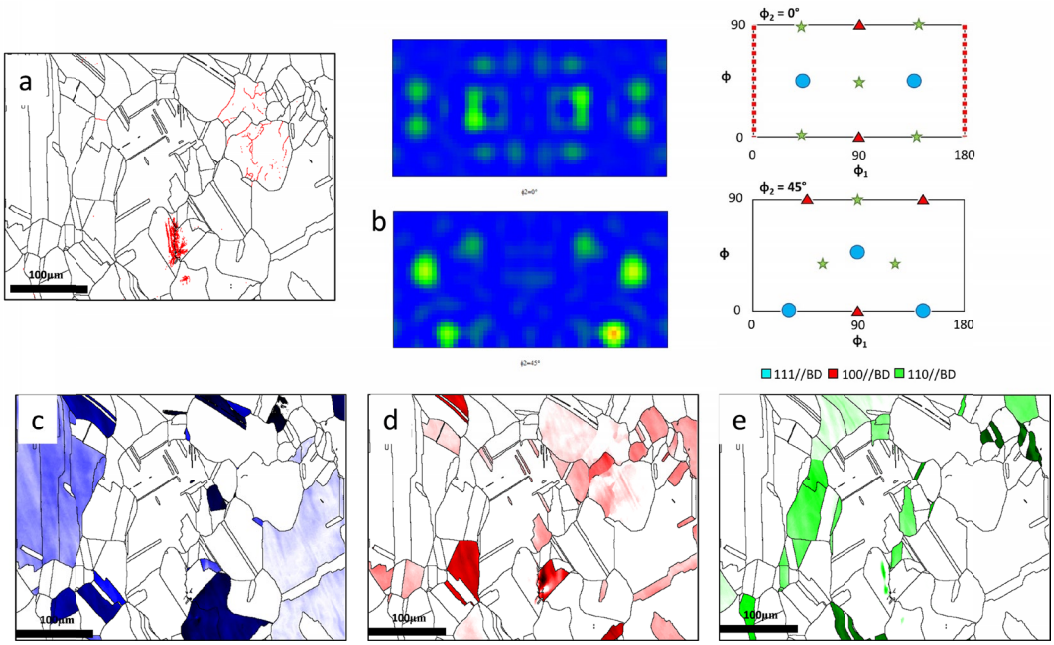

Fig. 2. The following figures are for HIP treated pure Ni sample, a) The grain boundary map with LAGB (red lines) and HAGB (black lines). b) The ODF maps displaying the section with $\varphi_2 = 0°$ (top) and $\varphi_2 = 45°$ (bottom). (The interpretation of the ideal orientations of ODF maps is shown in this figure legend. (c) 111 fiber, (d) 100 fiber and (d) 110 fiber texture

which is mixed with the intrinsic residual stress due to printing processes like static and dynamic recrystallization are initiated.

In contrast with the AP sample, there is strong crystallographic texture in the HIP, with 19.8 being the maximum intensity factor. It can be seen in Fig. 2b, at $\varphi_2 = 0°$, <111>||BD fiber texture is relatively dominant, whereas <100>||BD fiber texture has minor presence. At $\varphi_2 = 45°$, fiber textures <111>||BD and <110>||BD are present in dominance, whereas fiber texture <100>||BD has minor presence. Fig. 2(c-e) shows the ODF map illustrating the spatial distribution of various fiber textures. The presence of fiber texture c (35.9%) is in dominance along with the presence of <100>||BD (18.9%) and <110>||BD fiber textures (12.7%).

4. Evolution of texture

The evolution of texture as discussed in the previous section depends on the sample's processing history. There is an increase in the fraction of <111>||BD fiber texture after HIP treatment. This leads to a reduction in fiber texture <110>||BD in AP sample. The considerable rise in <111>||BD is directly attributable to the HIP deformation process. Due to this, there is grain rotation which develops <111>||BD texture [16]. Thus, a rise in <111>||BD fiber texture results in a considerable reduction in fiber texture <110>||BD.

4.1. Evolution of Twin Boundaries

It is well known that there is improvement in the mechanical properties after HIP. This exceptional arrangement of ductility with strength in the HIP sample is caused by various reasons like deformation twinning etc. It is expected that the present sample processed by HIP process would show higher mechanical properties as compared to the AP sample as the tensile properties of the present alloy is a part of future research. In the HIP sample, it can be seen from Fig. 2a that there is presence of twins in the microstructure. The HIP procedure involves application of 1 Mbar at a temperature of 1163°C for around 3 hours. The impact of this compression on the twins generation is examined as below.

Fig. 3 shows the twin boundary maps of AP and HIP sample. For the AP sample (Fig. 3a), the twin boundary map depicts negligible presence of CSL Σ3 boundaries (green colored lines). The CSL Σ3 boundaries of the microstructure can be seen are not lengthy and straight however appear comparable to other boundaries with high angle. The microstructure consists of marginal presence of other CSL boundaries and have a comparable structure, i.e., not lengthy and straight, rather are distributed randomly. The presence of CSL Σ3 boundaries is 4.61%, along with the presence of non CSL boundaries which have negligible presence in the microstructure, as seen in Fig. 1a.

Fig. 3b shows the twin boundary map of HIP sample. As observed in the microstructure, presence of the CSL boundaries in the microstructure is significant, especially Σ3. It can be observed that the boundaries appears in a annealing twins in a well-defined arrangement, i.e., existence of Σ3 boundaries in the coincidence site lattice structure [17]. The presence of the Σ3 boundaries is ~43.6%, and along with the presence of non CSL boundaries which have negligible presence in the microstructure.

The significant existence of twin (CSL Σ3) boundaries in the pure Ni HIP sample leads to definite impact on the mechanical properties of the element [18]. In the HIP process there is deformation to some extent therefore the occurrence of twinning due to deformation is expected. Pure Ni is a medium stacking

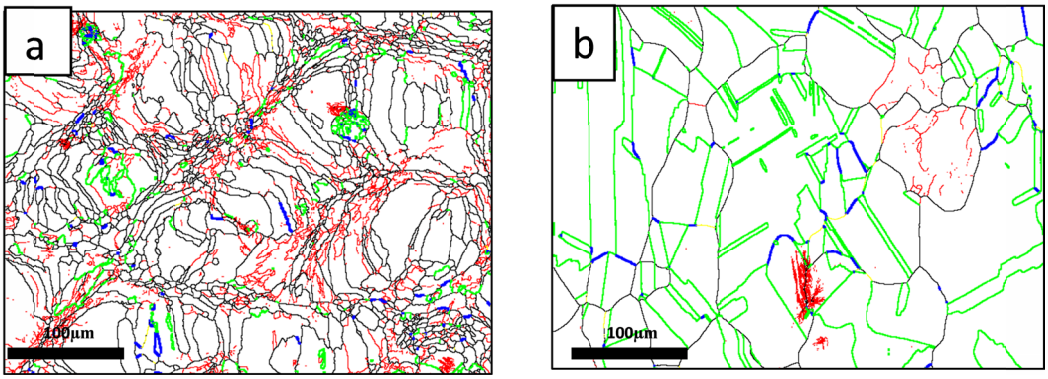

Fig. 3. CSL Σ3 boundaries map for (a) as printed and (b) HIP treated pure Ni sample. (Σ3-green, Σ5-red, Σ9-blue)

fault energy (SFE: 120-140 m J/m^2 [19]) element. Low-medium SFE promotes the dissociation of dislocations and the formation of stacking faults that limit cross slips [20], which finally favors deformation twinning. These twins promote great plasticity during further deformation [21,22].

Thus, it is envisaged that the presence of favorable fiber texture component and deformation twins would lead to higher mechanical properties of pure Ni sample fabricated by LPBF process.

5. Conclusions

On the basis of detailed microstructural analysis conducted on pure Ni fabricated by LPBF, the following conclusions can be drawn:

1. The sample of pure Ni (AP) contains predominantly <110>||BD fiber texture. On the other hand, the sample of pure Ni (HIP) contains <111>||BD grains. The formation of the texture <111>||BD was caused by the deformation linked with the HIP process which allowed the crystal to rotate.
2. A significant fraction of CSL Σ3 boundaries was observed in HIP sample is due to the medium stacking fault energy (SFE) of pure Ni.

Acknowledgments

The authors acknowledge the funding received from the New Brunswick Innovation Foundation (NBIF), Natural Sciences and Engineering Research Council of Canada (NSERC) and Canada Foundation for Innovation (CFI).

REFERENCES

[1] J.P. Kruth, M.C. Leu, T. Nakagawa, CIRP Annals-Manufacturing Technology **47** (2), 525-540 (1998).

[2] H. Fayazfar, M. Salarian, A. Rogalsky, D. Sarker, P. Russo, V. Paserin, E. Toyserkani, Materials & Design **144**, 98-128 (2018).

[3] H. Kumar, S.A. Khan, P.K. Arora, Indian Journal of Engineering and Materials Sciences (IJEMS) **28** (2), 115-124 (2021).

[4] S.N. Singh, S. Chowdhury, Y. Nirsanametla, A.K. Deepati, C. Prakash, S. Singh, L.Y. Wu, H.Y. Zheng, C. Pruncu, Materials **14** (4), 876 (2021).

[5] Y. Tian, K. Chadha, C. Aranas, Materials Science and Engineering: A **805**, 140790 (2021).

[6] Y. Tian, K. Chadha, S.H. Kim, C. Aranas, Materials Science and Engineering: A **805**, 140801 (2021).

[7] R. Palad, Y. Tian, K. Chadha, S. Rodrigues, C. Aranas, Materials Letters **275**, 128026 (2020).

[8] Y. Tian, R. Palad, L. Jiang, T. Dorin, K. Chadha, C. Aranas, Journal of Alloys and Compounds **885**, 161033 (2021).

[9] K. Chadha, Y. Tian, J. Pasco, C. Aranas, Materials Characterization **178**, 111285 (2021).

[10] S. Matsumoto, H. Kita, Nippon Steel & Sumitomo Metal Technical Report (106), 114-119 (2014).

[11] K. Chadha, Y. Tian, J. Spray, C. Aranas, Metals and Materials International **28**, 237-249 (2021).

[12] C. Wang, Q. An, Q. Niu, M. Chen, Journal of Materials 41-45 (2017).

[13] K. Geenen, A. Röttger, W. Theisen, Materials and Corrosion **68** (7), 764-775 (2017).

[14] A.A. Saleh, E.V. Pereloma, A.A. Gazder, Acta Materialia **61** (7), 2671-2691 (2013).

[15] A.T. English, G.Y. Chin, Acta Metallurgica **13** (9), 1013-1016 (1965).

[16] X. Wang, J.A. Muñiz-Lerma, O. Sánchez-Mata, M.A. Shandiz, M. Brochu, Materials Science and Engineering: A **736**, 27-40 (2018).

[17] H. Grimmer, W. Bollmann, D. Warrington, Acta Crystallographica Section A: Crystal Physics, Diffraction, Theoretical and General Crystallography **30** (2), 197-207 (1974).

[18] K. Chadha, Y. Tian, J.G. Spray, C. Aranas Jr, Metals **10** (6), 753 (2020).

[19] K.H. Lo, C.H. Shek, J. Lai, Materials Science and Engineering: R: Reports **65** (4-6), 39-104 (2009).

[20] M. Pham, S. Holdsworth, Materials Science and Engineering: A **556**, 122-133 (2012).

[21] O. Grässel, L. Krüger, G. Frommeyer, L. Meyer, International Journal of Plasticity **16** (10-11), 1391-1409 (2000).

[22] J.W. Christian, S. Mahajan, Progress in Materials Science **39** (1-2), 1-157 (1995).